Applied Catalysis B: Environmental 200 (2017) 121–132

Contents lists available at ScienceDirect

Applied Catalysis B: Environmental

journal homepage: www.elsevier.com/locate/apcatb

Direct reduction of nickel catalyst with model bio-compounds

Feng Cheng[a], Valerie Dupont[a,*], Martyn V. Twigg[b]

[a] School of Chemical and Process Engineering, The University of Leeds, Leeds LS2 9JT, UK
[b] TST Ltd., Caxton, Cambridge CB23 3PQ, UK

ARTICLE INFO

Article history:
Received 29 April 2016
Received in revised form 15 June 2016
Accepted 18 June 2016
Available online 23 June 2016

Keywords:
Nickel oxide
Bio-compounds
Catalyst reduction
Kinetics
Chemical looping

ABSTRACT

The effects of temperature and S/C on the reduction extent and kinetics of a steam reforming NiO/α-Al_2O_3 catalyst were systematically investigated using five bio-compounds commonly produced during the fermentation, pyrolysis and gasification processes of biomass (acetic acid, ethanol, acetone, furfural and glucose). Reduction was also performed with methane and hydrogen for comparison. Kinetic modelling was applied to the NiO conversion range of 0–50% using the Handcock and Sharp method. The two-dimensional nuclei growth model (A2) was found to fit very well except for glucose. For all the bio-compounds, the apparent activation energy of NiO reduction was between 30 and 40 kJ/mol. Their pre-exponential factors decreased in this order: CH_4 > ethanol ≈ acetone > acetic acid > furfural > glucose, probably due to the different activities of reducing species they produced. Optimal molar steam to carbon ratios for reduction kinetics were found between 1 and 2.

1. Introduction

The reduction of metal oxide is an important reaction in the fields of heterogeneous catalysis and metallurgy, the commonly used reducing agentsbeing either H_2, CO, CH_4 or carbon. Related reduction mechanisms have been investigated which normally involve surface adsorption, activation and radical formation [1–4]. The reduction kinetics are usually described using nucleation models or a shrinking core model [5]. With the development of DRI (direct reduction of iron ore) technology and the use of solid fuels in CLC, some solid carbonaceous materials such as coal, biomass and solid wastes have emerged as potential reducing agents. The understanding of the reduction mechanism is in progress but still far from completion. A two-step mechanism which involves the formation of reducing gases from solid carbonaceous materials and the regeneration of reducing gases by carbon gasification is usually suggested.

The chemical Looping Steam Reforming process has advantages over the conventional catalytic steam reforming process of internal heat supply, cyclic catalyst regeneration and easy integration with in situ CO_2 adsorption. In CLSR, whether the reforming fuel employed is able to reduce the oxygen carrier (supported metal oxide) at the beginning of fuel feed is critical to the subsequent steam reforming reaction. Previous studies in reduction of metal oxides used as oxygen transfer materials in CL processes mainly focused on screening suitable metal oxides based on their reduction reactivity with CH_4. It was found that supported NiO is a promising oxygen carrier in both Chemical Looping Combustion, a.k.a. CLC [6–8] and Chemical Looping Reforming [9] due to its good reduction reactivity and subsequent catalytic activity towards steam reforming reaction when using methane as the combustion fuel or hydrogen production feedstock. Reducibility of NiO/Al_2O_3 with hydrogen can be enhanced by adding alkali earth metal oxides to stabilize the support [10] or incorporating a second metal (e.g. Co) to form bimetallic oxygen carrier [11]. The carbon deposition occurring in the fuel reactor is another concern of a CL process. It was found that the carbon deposition depends on the nature of active metal oxide (Fe-based oxygen carrier has a less tendency to form carbon) and the availability of oxygen in the lattice of metal oxide or the surrounding atmosphere. Little is known of the ability or mechanisms of reduction of NiO under other reductants than H_2, CH_4, CO and NH_3. Recently, some renewable liquid feedstocks such as biomass pyrolysis oils (bio-oil) [12], ethanol supplemented by bio-oil [13], glycerol [14], vegetable oil [15], as well as non-renewable ones like used tyres pyrolysis oil [16] have been tested in chemical looping steam reforming conditions using NiO catalyst acting as both the oxygen transfer material and steam reforming catalyst. To the authors' knowledge, few studies have been devoted to the performance of individual bio-compound derived from bio-oil in a CL process, or specifically in the reduction of nickel oxide. The investigation on the reducing ability of bio-compounds, as well as their

* Corresponding author.
E-mail address: V.Dupont@leeds.ac.uk (V. Dupont).

http://dx.doi.org/10.1016/j.apcatb.2016.06.044

Nomenclature

A	pre-exponential factor in Arrhenius rate expression (Eq. (10)). Units depend on reaction model. Here A in s^{-1}
A2	Avrami–Erofeyev model of nucleation and nuclei growth with 2D (disc shape) nuclei, refers to solid state reactions
$C_{bio,g\ or\ S}$	gas concentration of bio-compound in bulk gas (g) or at particle's surface (S) in mol m^{-3}. (Eq. (7))
CL	chemical looping
CLC	chemical looping combustion
CLPO	chemical looping partial oxidation
CLSR	chemical looping steam reforming
d_p	catalyst particle size (assumed spherical = diameter), in m (Eqs. (6) & (9))
$D_{bio,N2}$	molecular diffusivity of relevant bio-compound in N_2 in $cm^2\ s^{-1}$ (Eq. (8)) and $m^2\ s^{-1}$ (Eq. (6))
D_e	effective diffusivity of bio-compound inside catalyst in $cm^2\ s^{-1}$ in Eq. (11) and $m^2\ s^{-1}$ in Eq. (10).
E_a	apparent activation energy in Arrhenius rate expression (Eq. (10)). Units depend on units of universal gas constant used in Eq. (10)
f	solid state conversion general function (Eq. (12))
g	solid state integral conversion general function (Eq. (13))
i	number of carbon atoms in bio-compound molecule
j	number of hydrogen atoms in bio-compound molecule
k_c	external mass transfer coefficient of bio-compound ($m\ s^{-1}$) to catalyst particle (Eq. (6))
l	number of oxygen atoms in bio-compound molecule
M_{bio}	molar mass of bio-compound $C_iH_jO_l$ ($g\ mol^{-1}$)
M_{H2}	molar mass of H_2 (=2.02 $g\ mol^{-1}$)
m	geometrical order in Eq. (14), (Hancock and Sharp's method) no units
n	molar flow rate of relevant species in mol s^{-1}
P	total pressure in atm (Eq. (8))
R	universal gas constant (e.g. 8.314×10^{-3} $kJ\ mol^{-1}\ K^{-1}$), Eq. (10)
$r_{bio,ext}$	chemical consumption rate of bio-compound per unit external surface area of catalyst in mol (of bio-compound) m^{-2} (of external spherical particle) s^{-1}. (Table 2)
r_{NiO}	chemical rate of NiO reduction in mol s^{-1}. (Table 2)
Re	Reynolds number (Eq. (5))
S/C	molar steam to carbon ratio
Sh	Sherwood number (Eq. (5))
Sc	Schmidt number (Eq. (5))
T	temperature in K (Eq. (8))
$v_{e,bio}$	atomic diffusion volume for relevant bio-compound (Eq. (8))
$W_{bio,r}$	molar flux of bio-compound at catalyst particle's external surface mol $m^{-2}\ s^{-1}$. (Eq. (7))
X	conversion fraction or percent conversion of relevant reactant, e.g. X_{bio} (Eq. (2)) and X_{H2O} (Eq. (3))
y	molar fraction of relevant species in the dry outlet gas: $y_{C_2} = y_{C_2H_4} + y_{C_2H_6}$; $y_{C_3} = y_{C_3H_6} + y_{C_3H_8}$. The subscript 'dry', 'in', and 'out' refer to conditions following water removal, at reactor inlet and outlet, respectively

Nomenclature

Greek symbols

α	extent of NiO reduction moles of NiO converted to Ni/initial moles of NiO
β	constant in Eq. (14)
ε	stoichiometric number of moles of NiO reduced by 1 mol of bio-compound according to reaction R1. (Table 2, Eq. (9))
Φ_p	catalyst particle's porosity (void fraction), no units, (Eq. (11))
Φ_n	Thiele modulus, no units, Eq. (10)
σ_c	constriction factor of catalyst, no units, (Eq. (11))
τ	tortuosity factor of catalyst, no units, (Eq. (11))

influence on the catalytic activity of reduced metal oxide, is rare in the literature, but quite significant to the potential application of bio-oil in a CL process.

The direct reduction of 18 wt% nickel oxide steam reforming catalyst supported on α-alumina by reforming fuel acetic acid during a steam reforming process was investigated in [17]. Steam reforming of acetic acid took place as soon as metallic Ni was produced from NiO reduction by the acetic acid. There are several materials-related parameters that may influence the reduction of NiO, such as the presence of other metals or choice of support. In the present study we focus on the nature of the reducing agent, while choosing the simplest of NiO steam reforming catalysts, i.e. 18 wt% NiO on α-Al_2O_3 (Johnson Matthey) as the oxide, given its proven ability to auto-reduce using acetic acid, as well as ethanol and bio-oils [13,18]. In addition to carboxylic acids, alcohols, ketones, furans and sugars are common chemical families present in the bio-oils and bio-crudes produced by the fast pyrolysis or other liquefaction processes of land-grown and aquatic biomass. The reduction using compounds derived from biomass may potentially be a more complicated process in which many species (e.g. bio-compound itself, decomposition intermediates, reforming products H_2 and CO) may be involved. Thus, the auto-reduction of 18 wt% NiO/α-Al_2O_3 steam reforming catalyst with ethanol, acetone, furfural and glucose is studied here with emphasis on comparing the reducing ability and reduction kinetics of bio-compounds each representing a different functional group. Furthermore, the model bio-compounds chosen here are key players in bio-refinery operations, either as platform chemicals, building blocks, intermediates or valuable end products which introduce a renewable route to the production of green solvents, resins, acetates, food additives, and cosmetics. This study aims to demonstrate the dependence of extent of reduction and reduction rate on the type of bio-compounds, temperature, and steam content present in the reduction system. Forthcoming publications will focus on the subsequent catalytic activity of the steam reforming reaction and stability of outputs under CL-SR conditions following auto-reduction.

2. Materials and methods

2.1. Materials

The catalyst used in this project was 18 wt% NiO supported on α-Al_2O_3 (NiO/α-Al_2O_3), supplied in raschig rings form by Johnson Matthey Plc. It had a bulk density of 1201 kg m^{-3}, and average crush strength of 735 N. The NiO/α-Al_2O_3 catalyst pellets were crushed and sieved to particle size of 1.0-1.4 mm prior to being used in reduction experiments in a packed bed reactor. Onene experiment (ethanol, S/C 3, 650 °C) also used particle size of ~0.1 mm to rule out mass transfer limitations. The 1.0-1.4 mm size fresh catalyst

Table 1
Feed rates of liquid feedstock into the packed bed reactor.

Reductant	C feed rate (mmol/min)	Fuel feed (ml/min)	Solution of fuel and water (ml/min)			
			S/C1	S/C2	S/C3	S/C5
acetic acid	1.1749	0	0.0552	0.0768	0.0984	0.1416
ethanol	1.1732	0	0.0558	0.0774	0.0990	0.1422
acetone	1.1755	0	0.0503	0.0719	0.0935	0.1367
furfural	1.1740	0.0194	n/a (fuel insoluble)	0.0424	0.0637	0.1061
			S/C4.5	S/C6	S/C7.5	S/C9
glucose	0.6061	0	0.0636	0.0750	0.0966	0.1100

particles had a BET surface area of 2.3 m^2/g with BJH pore size of 2.5 nm (Quantachrome Instrument Nova® 2200). The crystallite size of the fresh NiO catalyst crystallite was 45 nm, determined by powder XRD coupled with Rietveld refinement (Bruker D8 X-Ray diffractometer, with HighScore Plus software from PANalytical, see Section 2.5) [18].

Blank α-Al_2O_3 pellets, provided by TST Ltd, were crushed into the same particle size for the use in control experiments.

The bio-compounds used in packed bed reactor experiments include acetic acid, ethanol, acetone, glucose and furfural. These represent five common functionalities of the organics present in bio-oils and bio-crudes (acids, alcohols, ketones, sugars and furans). In addition, glucose (α-D-glucopyranose, a.k.a. D-glucose) was chosen to represent solid bio-compounds. D-Glucose is the basic building block of cellulose, a major component of biomass (along with lignin and hemicellulose). All the bio-compounds used had a purity of >99%. Acetic acid, ethanol and furfural were purchased from Sigma-Aldrich, and acetone and D-glucose (anhydrous) were obtained from Fisher Scientific.

2.2. Experimental set-up and operation procedure

The packed bed reactor set-up used in this project was composed of six functional modules: reactor, liquid feeding, gas feeding, temperature control, cooling system and outlet gas analysis. The reactor was made of quartz with an inner diameter of 12 mm and the length of 49.5 cm, with a quartz fritter located a mid-length to hold the catalyst. It was manufactured by Yorlab Company (UK). During experiments, the reactor was held inside a tube furnace (Elite Thermal Systems Ltd. TSV12/50/300). The temperature of the furnace was regulated by a Eurotherm 2416 temperature controller. The temperature of the reactor, which may be slightly different from that of the furnace, was monitored in real-time by a K-type thermocouple. A diagram of the experimental set-up can be found in [17]. The reaction temperature mentioned hereafter refers to the reactor temperature. The liquid feeding (the injection of bio-compounds and water into the reactor) was performed by programmable syringe pumps (New Era Pump Systems). The gas feeding to the reactor was controlled by MKS mass flow rate controllers. The gaseous products from the reactor were cooled down by a condenser. A coolant (ethylene glycol and water in volume ratio of 1:1) at −5 °C was circulated between the condenser and a chiller (Fisher Scientific 3016S) to maintain the condenser at a low temperature.

For the bulk of the experiments, 2 g of fresh catalyst were placed in the middle of the quartz reactor. The 2 g of catalyst typically occupied 2 mL volume in the reactor. Around 1.7 g of α-Al_2O_3 balls (3 mm in diameter) were added on the top of the catalyst bed as pre-heater when using furfural as feedstock. For the other bio-compounds, no precautions were taken below or above the catalyst bed. One experiment, for ethanol feed and reactor at 650 °C at S/C of 3, was carried out using 1 g of catalyst to study mass transfer limitations. The experimental process was carried out at atmospheric pressure under a continuous N_2 flow of 200 sccm in all experiments and in the absence of air. When the reactor was heated to a set temperature, the liquid feed was fed into the reactor at a given flowrate (Table 1). For water-soluble bio-compounds (acetic acid, ethanol, acetone and glucose), an aqueous solution of bio-compound was made first and then injected into the reactor by one syringe pump. Different molar steam to carbon ratios (S/C) were achieved by changing the molar ratio of water to bio-compound in the solution. The insoluble bio-compound furfural and water were fed into the reactor separately by two separate syringe pumps. Different S/C ratios were then achieved by setting the flow rates of furfural and water. The flow rate of carbon equivalent (the flow rate of bio-compound multiplied by the number of carbon atoms in the bio-compound molecule) was kept at around 1.174 mmol/min for all the bio-compounds except for glucose (see Table 1). Previous studies [19,20] reported that the steam reforming of glucose had a larger tendency to form coke and required higher S/C ratios than other bio-compounds. Therefore, the carbon equivalent input of glucose in this project was 0.6061 mmol/min and the S/C ratio (4.5–9) investigated was larger than that for the other bio-compounds (1–5).

2.3. Reactor effluents analysis

Condensable gas products and unreacted water were trapped in a condensate collector, with any residual moisture later removed by silica gel. The composition of the dry outlet gas was measured with an Advanced Optima gas analyser from ABB and recorded online at 5 s intervals. The ABB gas analyser consisted of two analyser modules: Uras 14 and Caldos 15. The Uras 14 was capable of detecting CH_4, CO_2 and CO based on infrared absorption principle. The Caldos 15 was used for H_2 measurement by thermal conductivity. A Varian micro gas chromatograph GC, equipped with MS5 and PPQ columns was used following the ABB gas analyser to detect other possible hydrocarbon gases C_2 (C_2H_4, C_2H_6) and C_3 (C_3H_6, C_3H_8). Both MS5 and PPQ columns were equipped with thermal conductivity detectors (TCD).

2.4. Elemental balance and definition of process outputs

In a typical packed bed experiment, the general reduction reactions of NiO in the presence of steam by an organic compound of elemental formula $C_iH_jO_l$ can be expressed by R1 (CO_2 and H_2O products, a.k.a. chemical looping combustion, or CLC) and R2 (CO and H_2 products, a.k.a. chemical looping partial oxidation, or CLPO), while steam reforming (R3), and water gas shift (R4), which require metal catalyst, are activated when the NiO reactant has undergone sufficient reduction to Ni.

$$(2i + 0.5j - l)NiO + C_iH_jO_l \rightarrow (2i + 0.5j - l)Ni + iCO_2 + 0.5jH_2O \quad (R1)$$

$$(i - l)NiO + C_iH_jO_l \rightarrow (i - l)Ni + iCO + 0.5jH_2 \quad (R2)$$

In R1 and R2, combinations of *i*, *j*, and *l* can take values so as to include C, H_2, CO, CH_4 as well as values representing unreacted bio-compound and intermediates as the reductants.

$$(i - l)H_2O + C_iH_jO_l \leftrightarrows iCO + (i + 0.5j - l)H_2 \quad (R3)$$

$$CO + H_2O \leftrightarrows CO_2 + H_2 \quad \text{(R4)}$$

The initial data include:

(1) The molar fraction of CO_2, CO, CH_4, and H_2 in the dry outlet gas measured with ABB gas analyser
(2) The molar fraction of C_2 (C_2H_4, C_2H_6) and C_3 (C_3H_6, C_3H_8) hydrocarbons in the dry outlet gas measured with micro GC
(3) The feed flow rates of water, carrier gas N_2, and bio-compound
(4) The mass of the catalyst used in each run and the NiO loading in the catalyst

Process outputs include:

(1) The reduction rate of NiO to Ni
(2) The conversion fraction of water or bio-compound
(3) Individual C-containing and H-containing gas yields

These data could be obtained through elemental balance calculation and some reasonable assumptions [15]. Related parameter symbols are defined in the nomenclature at the end of this paper.

The molar flow rate of total dry outlet gas ($n_{out,dry}$) was estimated based on nitrogen balance (Eq. (1)). The molar feed flow rate of N_2 (n_{N2}) was maintained at 1.386×10^{-4} mol s^{-1}, equivalent to a volume flow rate of 200 sccm (sccm or standard cubic centimetre per minute = cm^3 min^{-1} at 293 K and 1 atm) during the experimental process.

$$n_{out,dry} = \frac{n_{N_2}}{1 - y_{CH_4} - y_{CO} - y_{CO_2} - y_{H_2} - y_{C_2} - y_{C_3}} \quad (1)$$

The yield of each gas product is defined as the molar rate of gas produced, and equals the dry gas mol fraction in the gas products y, measured by online analysers or micro GC, and multiplied by $n_{out,dry}$ from the N elemental balance expressed in (Eq. (1)).

The conversion fraction of bio-compound (X_{bio}) to gases was calculated based on a carbon balance, dividing the total molar flow of carbon in the gaseous products by the molar flow of carbon in feed, as described in Eq. (2).

$$X_{bio} = 100\frac{n_{out,dry} \times \left(y_{CO} + y_{CO_2} + y_{CH_4} + 2y_{C_2} + 3y_{C_3}\right)}{i \times n_{bio,in}} \quad (2)$$

The H_2O conversion fraction (X_{H2O}) during reduction is calculated on a basis of hydrogen balance (Eq. (3)) and using as input the value of X_{bio} found using Eq. (2).

$$X_{H_2O} = 100\frac{n_{out,dry} \times (4y_{CH_4} + 2y_{H_2} + 4y_{C_2H_4} + 6y_{C_2H_6} + 6y_{C_3H_6} + 8y_{C_3H_8}) - j \times n_{bio,in} \times X_{bio}}{2n_{H_2O,in}} \quad (3)$$

On the basis of an oxygen balance, Eq. (4) was used to estimate the rate of NiO reduction to Ni. Equation (4) requires as inputs $n_{out,dry}$, X_{H2O} and X_{bio} from Eqs. (1)–(3).

$$\text{NiOred.rate} = n_{out,dry} \times \left(y_{CO} + 2y_{CO_2}\right) - n_{H_2O,in} \times X_{H_2O} - l \times n_{bio,in} \times X_{bio} \quad (4)$$

The total moles of NiO reduced to Ni over a given duration (time on stream) were obtained from the time integration of the above rate equation. α, the conversion extent of NiO to Ni (or 'extent of reduction') was then shown as a fraction or percentage of the initial moles of Ni present in catalyst.

The reduction process was carried out in a packed bed reactor at an approximately constant temperature (isothermal reduction). The fresh catalyst load of 2 g of 18 wt% NiO/α-Al_2O_3 in all experiments, was placed in the middle of the reactor for reduction. Like acetic acid, ethanol, acetone, and glucose were individually dissolved in water to make solutions with a given molar steam to carbon ratio (S/C), prior to being fed into the reactor. Furfural and water were injected to the reactor separately as furfural is insoluble. The reduction of fresh catalyst by H_2 was also conducted in the packed bed reactor using 5% H_2/N_2 gas at a flow rate of 300 sccm in the absence of steam. 10% CH_4/N_2 gas with a flow rate of 222 sccm was used to study the reduction of fresh catalyst by CH_4. Water was fed into the reactor by syringe pump (S/C=3) before the feed of CH_4 started, similarly to the recommended start-up procedure when using natural gas to reduce reforming catalyst in a commercial operation [21].

Each run of experiment proceeded for a total of 45 min, although the reduction process was shown to be completed in the first 600 s of the first gases being detected for all the bio-compounds tested. Molar fractions of gaseous products from the reactor were used to calculate the NiO reduction rate on the basis of the oxygen elemental balance (Eq. (4)).

2.5. Reactor material analysis

After the experiments, the catalysts were collected for characterisation with powder XRD, and the composition of reacted catalysts was derived from the XRD data using Rietveld refinement [22]. XRD tests were performed on an X-ray diffractometer (D8 from Bruker). A voltage of 40 kV and a current of 40 mA were applied to the X-ray generator of Cu Kα1 radiation (1.54060 Å) and Cu Kα2 radiation (1.54443 Å). The scanning range (2θ) of X-rays was from 20° to 80° with an increment of 0.0332°/step and a speed of 0.7 s/step. The sample was crushed to fine powder prior to XRD tests. The XRD patterns obtained were used for phase analysis and composition analysis. Both analysis were conducted using the X'Pert HighScore Plus software from PANalytical. Rietveld refinement is a full-pattern fit method and able to deal reliably with strongly overlapping reflections, yielding mass percentage of each crystalline substance in the sample. ICDD reference patterns 04-005-4505, 04-010-6148, and 04-013-0890 were selected for phases of α-Al_2O_3, Ni and NiO, respectively, during Rietveld refinement, as they matched with the diffraction peaks experimentally observed. The quality of the refinements was gauged by weighted R profile (R_{wp}) and goodness of fit (GOF). A refinement with R_{wp} less than 10 and GOF less than 4 could be considered as good [22,23]. All the Rietveld refinements shown in the present study satisfied this requirement. Using these XRD facilities, a previous study of ours determined that the fresh catalyst contained, in agreement with the manufacturer's data (JM), 17.8 wt% of crystalline NiO on α-Al_2O_3 and no metallic Ni, and confirmed lack of amorphous material Ni/NiO/Al_2O_3 [24].

3. Results and discussion

3.1. Maximum extent of reduction

The maximum extent of reduction of a metal oxide catalyst, i.e. the maximum percentage of its oxide store that can be reduced in practice, is influenced by various factors including the chemical nature of the catalyst support, the reduction temperature and duration, and the composition of reducing gas [25,26]. According to the literature [26], when the reduction was carried out with pure H_2, the optimal temperature was found to be around 600 °C. Below this temperature the reduction was slow and incomplete. Above this temperature, some sintering may take place, which lowered the nickel surface area. Therefore, when using bio-compounds to reduce the NiO catalyst, it is also important to find out such an optimal temperature which could lead to the largest extent of reduction but no sintering.

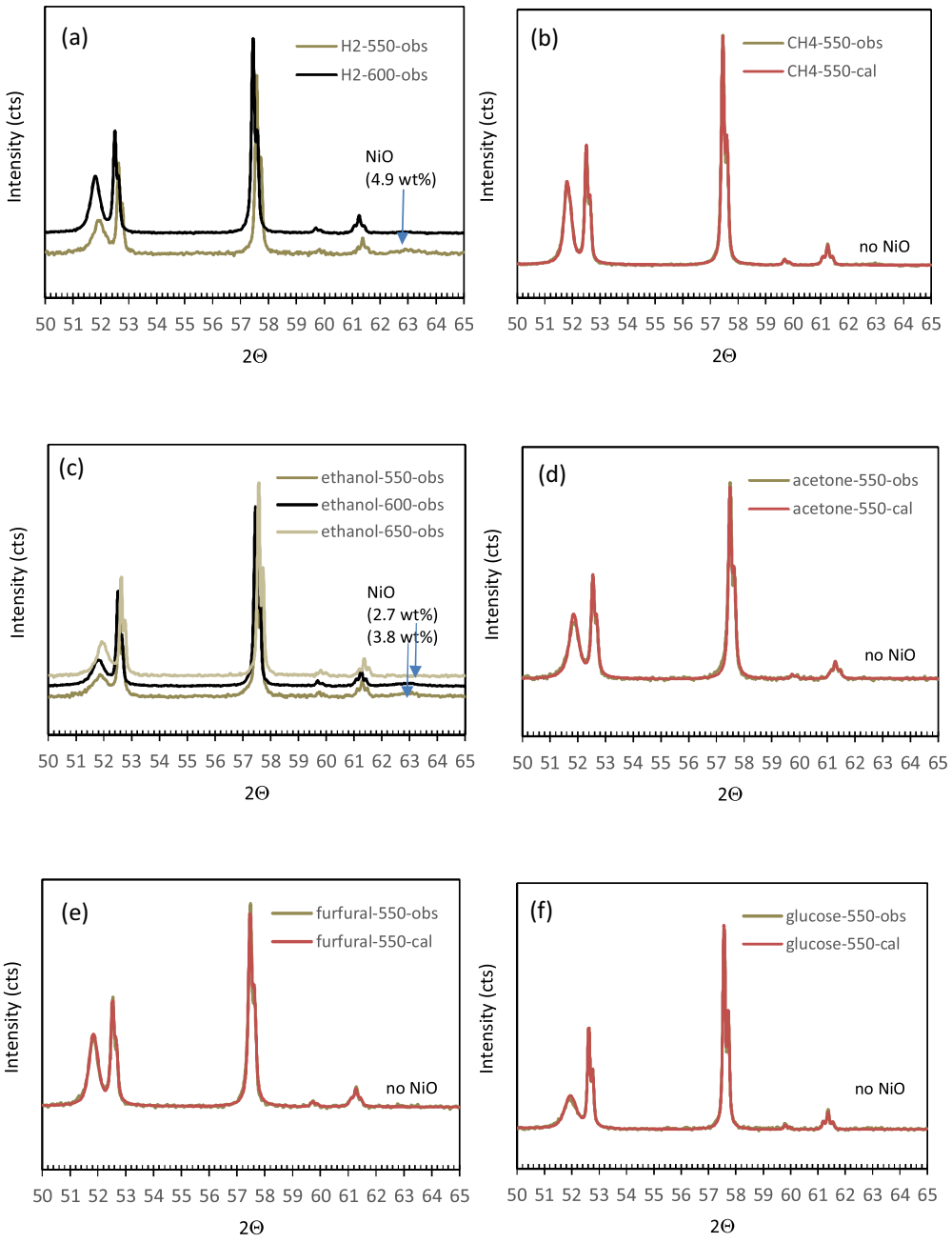

Fig. 1. XRD patterns (observed) and Rietveld refinement (calculated) results of catalysts after reduction with (a) H_2 and (b) methane, (c) ethanol, (d) acetone, (e) furfural, and (f) glucose. S/C=3 was used for all these reductants except glucose (S/C=6), and H_2 (no steam).

Fig. 1 shows the XRD profiles of the catalyst reacted with hydrogen (1a), methane (1b), and bio-compounds (1c-1f) in the temperature range 550–650 °C and the 2 theta range of 50–65°, using S/C of 3 except for glucose (S/C = 6) and H_2 (no steam) in order to identify clearly the characteristic diffraction peak of NiO (at 2 theta ~62.9°). Fig. 1(a–f) all display XRD spectra devoid of amorphous content, as evidenced by the flat baselines obtained in all the cases, with distinct sharp peaks. When subjecting the catalyst to ethanol vapour at 550 °C, the reduction of NiO to Ni occurred, demonstrated by the appearance of Ni diffraction peaks. However, the reduction was not entirely complete, as 3.8 wt% NiO remained in the sample. When using the other reductants, similar XRD profiles were obtained. The difference among them was whether the NiO peaks persisted. Apart from the three phases α-Al_2O_3, NiO, and Ni, there was no evidence of other phases (e.g. graphite), nor amorphous content (flat baseline maintained). A distinct NiO peak was observed in the XRD profile of the catalyst reduced with H_2 at 550 °C (2a), which accounted for 4.9 wt% of the catalyst. The NiO peak disappeared at 600 °C, indicating a complete conversion of NiO to Ni. When using ethanol as reductant, the intensity of the NiO peak at 62.9° decreased as the reduction temperature rose and the absence of this peak was observed at 650 °C (2c). This result confirmed that the maximum reduction extent was affected by temperature. Compared to the reduction with H_2 or ethanol, the catalyst reductions with CH_4, acetone, furfural or glucose achieved complete reduction at a lower temperature (550 °C).

In summary, NiO catalyst could be completely reduced by ethanol at 650 °C and by acetic acid [17], acetone, furfural or glucose at 550 °C. To find out the influence of different reducing agents

on Ni surface area (Ni dispersion), a further characterisation such as H_2 chemisorption [27] would be required.

3.2. Mass transfer limitations considerations

The reduction of NiO catalyst with bio-compound vapour is a type of gas-solid reaction. The global reduction kinetics may be controlled by one of the following steps [28,29]: diffusion of bio-compound vapour through gas phase to the exterior of particles (external mass transfer), diffusion into the porous particles (internal mass transfer), product-layer diffusion, or chemical reaction with NiO to produce Ni. Chemical reduction itself may be a complex process, potentially consisting of several steps. The reduction mechanism of supported NiO with H_2 was proposed as follows [29]: (1) dissociation of H_2 to form adsorbed H radicals (initially by NiO, then by newly formed Ni), (2) surface diffusion of H radicals to a reduction centre, (3) rupture of Ni—O bonds to produce Ni atoms, (4) nucleation of Ni atoms into metallic Ni clusters, and (5) growth of Ni clusters into crystallites. Any one or combination of these steps, together with the removal of water, may control the overall reaction rate. When using bio-compounds, the reduction process may become more complicated because of the availability of various reducing species (bio-compound, decomposition intermediates, H_2, CO, CH_4, transient C etc.), and the competition from steam reforming. Nonetheless, these basic steps including dissociative adsorption, surface diffusion of radicals, rupture of Ni—O bonds, nucleation and nuclei growth are believed to be common to different reductants. In this section, the influences of external mass transfer and internal mass transfer on the global reduction rate were checked.

3.2.1. External mass transfer

Normally, the external diffusion resistance could be reduced as much as possible by using high gas flow and small mass of solid sample. In this work, the reduction rate (in $mol\,s^{-1}$) was halved when decreasing the mass of NiO catalyst from 2 g to 1 g using an ethanol-water mixture at S/C of 3, indicating the external diffusion resistance was not significant. Additionally, the theoretical molar fluxes of bio-compound vapour ($W_{bio,r}$) at the external surface of the catalyst particles were estimated, similarly to [30]. Reynolds numbers were estimated for all the experiments at 650 °C, and were in the range 3.4-3.7 for all mixtures. This was found using feed mixtures (bio-compound/H_2O/N_2) densities ranging 0.362-0.478 $kg\,m^{-3}$ and assuming the dynamic viscosity of the feeds was represented by that of N_2 and steam since the two species were in highest feed concentrations (69–72 vol% N_2, 23–27 vol% H_2O), with $\mu_{N2}=3.94\times10^{-5}\,kg\,m^{-1}\,s^{-1}$, $\mu_{steam}=3.46\times10^{-5}\,kg\,m^{-1}\,s^{-1}$ at 650 °C. The particles' diameter d_p was averaged at 1.2 mm, and inter-particle velocities were calculated to range from 0.274 to 0.327 $m\,s^{-1}$ for all the feed mixtures. In these conditions, the Ranz and Marshall equation for mass transfer in laminar flow around a sphere could be used to characterise the external mass transfer around the individual catalyst particles [31]:

$$Sh = 2 + 0.6Re^{1/2}Sc^{1/3} \quad (5)$$

$$k_c = \frac{D_{bio,N_2}}{d_p} Sh \quad (6)$$

$$W_{bio,r} = k_c \left(C_{bio,g} - C_{bio,S}\right) \quad (7)$$

Where *Sh*, *Sc* and *Re* are the Sherwood number, the Schmidt number and the Reynolds number, respectively, k_c is defined as the external mass transfer coefficient ($m\,s^{-1}$). $D_{bio,N2}$ is the molecular diffusivity of the bio-compound in the bulk gas mixture ($m^2\,s^{-1}$). Here the bulk gas is assumed to consist of N_2, given its prevalence in the feeds. Values for $D_{bio,N2}$ were determined using the methodology

Table 2
Determination of external mass transfer rate $W_{bio,r}$ compared to chemical consumption rate r_{bio} of bio-compound (and methane) at catalyst particle's external surface at 650 °C, 1 atm, S/C of 3 (except glucose for which S/C is 6). Large ratio of $W_{bio,r}/r_{bio}$ (≫1) indicates external mass transfer is not rate limiting. Determination of Thiele modulus Φ_n inside catalyst particle, small Φ_n (≪1) indicates internal diffusion is not rate limited.

Bio-compound $C_iH_jO_l$	methane CH_4	acetic acid $C_2H_4O_2$	ethanol C_2H_6O	acetone C_3H_6O	furfural $C_5H_4O_2$	Glucose $C_6H_{12}O_6$
External mass transfer calculation	S/C = 3 (S/C = 6 glucose), 650 °C, 1 atm, 2 g catalyst, d_p 1.2 mm, feed flows in Table 1, cat. bulk density 1.201 $g\,cm^{-3}$, cat. Vol bed 1.67 cm^3, nb particles ~1162					
diffusion volume v_{bio}	24.42	51.88	50.36	66.86	81.18	135.44
$D_{bio,N2}$ in $cm^2\,s^{-1}$	1.593	0.880	0.932	0.800	0.690	0.524
gas density mixture feed in $kg\,m^{-3}$	0.362	0.413	0.388	0.396	0.430	0.479
Reynolds number	3.61	3.65	3.43	3.40	3.60	4.00
Schmidt number	6.84×10^{-4}	1.08×10^{-3}	1.09×10^{-3}	1.24×10^{-3}	1.33×10^{-3}	1.57×10^{-3}
Sherwood number	2.10	2.12	2.11	2.12	2.13	2.14
mass transfer coef. k_c ($m\,s^{-1}$)	2.79×10^{-1}	1.55×10^{-1}	1.64×10^{-1}	1.41×10^{-1}	1.22×10^{-1}	9.34×10^{-1}
$C_{bio,g}$ in $mol\,m^{-3}$	1.082	0.607	0.606	0.411	0.249	0.107
$Min\,C_{bio,S}$ in $mol\,m^{-3}$	Negl.	Negl.	Negl.	0.123	0.057	0.014
$W_{bio,r}$ in $mol\,m^{-2}\,s^{-1}$	3.02×10^{-1}	9.43×10^{-2}	9.96×10^{-2}	4.06×10^{-2}	2.3×10^{-2}	8.70×10^{-3}
ε (=2i+0.5j-l) in mol NiO/mol bio via R1	4	4	6	8	10	12
$r_{bio,ext}$ in $mol\,m^{-2}\,s^{-1}$ (ext. surface of sphere)	2.40×10^{-3}	1.28×10^{-3}	1.28×10^{-3}	7.88×10^{-4}	3.89×10^{-4}	3.15×10^{-4}
ratio $W_{bio,r}/r_{bio}$	122	72	76	50	58	27
intraphase mass transfer calculation	$\sigma_C = 0.8$, $\tau = 3.54$, $\Phi_p = 0.59$, model Avrami–Erofeyev 2D					
D_e in $cm^2\,s^{-1}$	0.212	0.117	0.124	0.107	0.092	0.070
$C_{bio,S}$ at $\alpha = 0.5$ in $mol\,m^{-3}$	0.541	0.303	0.303	0.205	0.124	0.054
$k_{NiO\rightarrow Ni}$ (Section 3.5) in s^{-1}	0.0136	0.0074	0.0103	0.0088	0.0045	0.0033
Max rate bio. cons. (model A2) $mol\,m^{-3}\,s^{-1}$	6.11×10^{-3}	1.87×10^{-3}	1.72×10^{-3}	7.52×10^{-4}	1.87×10^{-4}	4.91×10^{-5}
Thiele modulus Φ_n	1.61×10^{-2}	1.60×10^{-2}	1.50×10^{-2}	1.30×10^{-2}	8.94×10^{-3}	8.02×10^{-3}

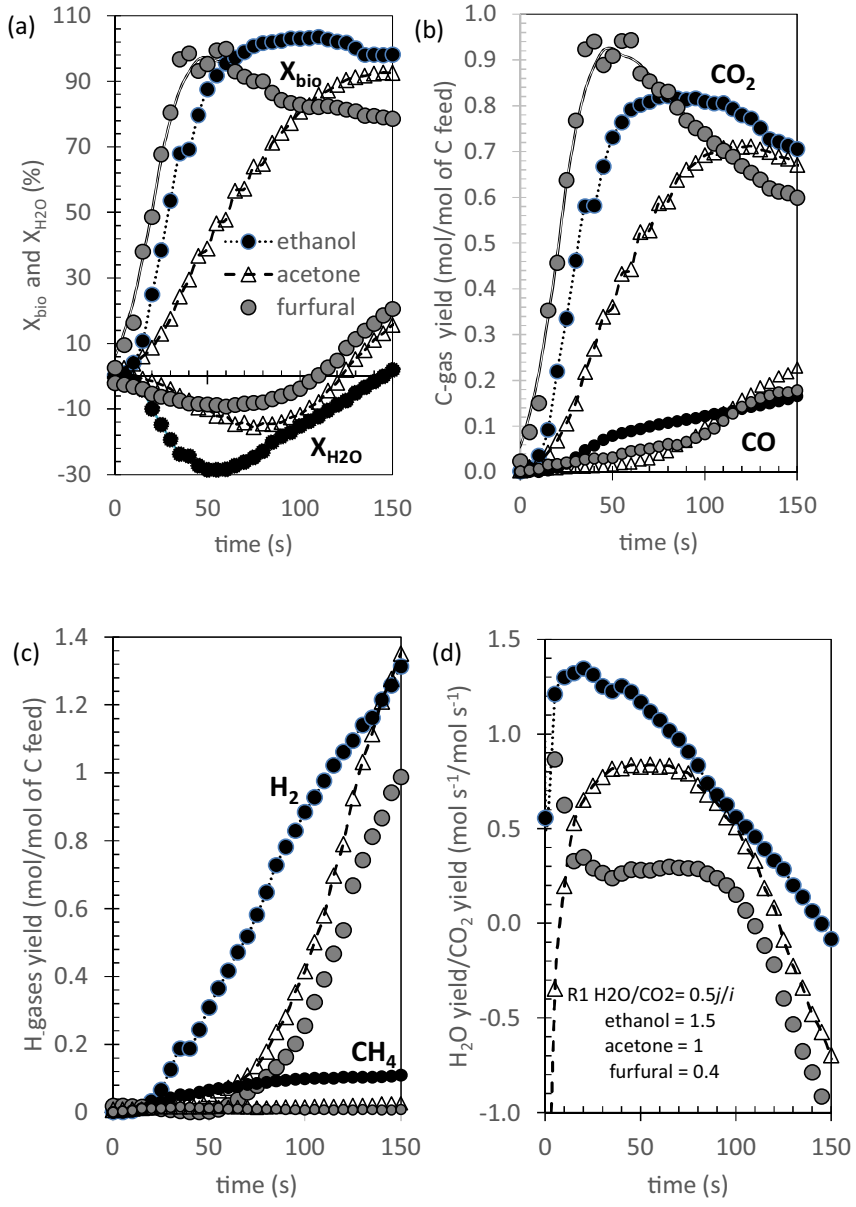

Fig. 2. Main outputs with time on stream for C-feed = 1.174 mmol/min, S/C=3, 650 °C, 2 g catalyst. (a) Percent bio-compound conversion X_{bio} (top curves, Eq. (2)) and steam conversion X_{H2O} (bottom curves, Eq. (3)), $X_{H2O} < 0$ steam is a net reaction product, (b) Yields of CO_2 (top) and of CO (bottom), (c) Yields of H_2 (top) and CH_4 (bottom) (d) ratio of yields of H_2O to CO_2 product, when >0 indicates H_2O is net reaction product. Insert in (d) lists maximum values 0.5 *j*/*i* according to reduction reaction R1.

described in [32] for estimation of binary gas phase diffusion coefficients for any organic species. The equation derived in [32] and used here was

$$D_{bio,N_2} = \frac{1.00\times10^{-3}T^{1.75}\left(1/M_{bio}+1/M_{N_2}\right)^{1/2}}{P\left[\left(\sum_{bio} v_{e,bio}\right)^{1/3}+(17.9)^{1/3}\right]^2}, \quad (8)$$

which produces $D_{bio,N2}$ in $cm^2\,s^{-1}$, where T is the temperature in K, M the relevant molar masses in $g\,mol^{-1}$, P the total pressure in atm. 17.9 is the diffusion volume of N_2 and $v_{e,bio}$ the atomic diffusion volumes for an atom of type e. For instance, here atoms e in the bio-compound are either C, H or O, with $v_C = 16.5$, $v_H = 1.98$, $v_O = 5.48$, $v_{ring} = -20.2$, in which case $v_{C2H6O} = 2\times16.5 + 6\times1.98 + 1\times5.48 = 50.36$, thus yielding $D_{ethanol,N2}$ at 650 °C and 1 atm of 0.932 cm^2/s. Values of $D_{bio,N2}$ were found to vary according to feedstock due to the differences in molar masses in bio-compounds and atomic diffusion volumes. Parameters for this calculation are included in Table 2. In Eq. (7), $C_{bio,g}$ and $C_{bio,S}$ are the concentrations of bio-compound in the bulk gas phase and on the catalyst's external particle surface ($mol\,m^{-3}$), respectively. Concentrations were determined using the ideal gas law, with $C_{bio,g}$ the feed value and $C_{bio,s}$ estimated using the maximum bio-compound conversion, which would have resulted in maximum external mass transfer rate.

The parameters for the calculation $W_{bio,r}$ (in $mol\,m^{-2}\,s^{-1}$) for the different bio-compounds' feed mixtures are summarized in Table 2. External mass transfer can be ruled out as rate-limiting when $W_{bio,r}$ is much larger than the maximum chemical rate of bio-compound consumption per unit of external area of particle ($r_{bio,ext}$). The latter is determined at 650 °C and S/C of 3 (except 6 for glucose) using Eq. (9) which assumes a spherical particle shape,

$$r_{bio,ext} = \frac{r_{NiO}\text{ at the peak of rate curve(mol/s)}}{\text{nb particles in reactor}\times\pi(d_p)^2\times\varepsilon} \quad (9)$$

Where the number of particles present in the bed is approximated to a maximum of 1162, based on the ratio of bed volume (1.67 cm^3)

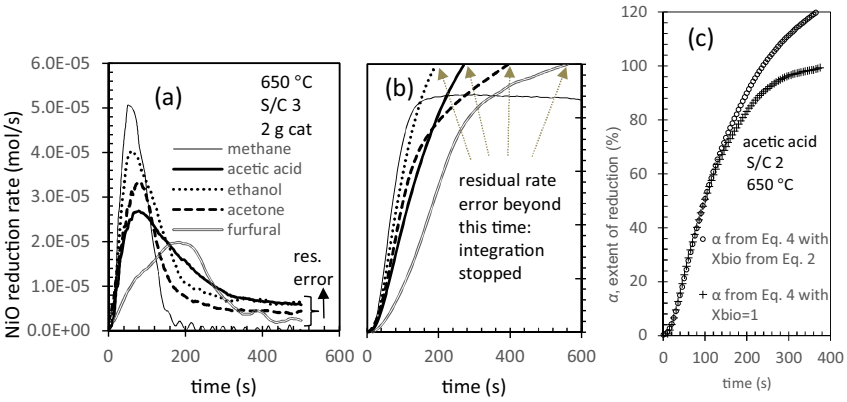

Fig. 3. (a) Reduction rates of 2 g of 18 wt% NiO/α-Al_2O_3 under methane, acetic acid, ethanol, acetone and furfural (molar carbon feed rate bio-compound 1.174 mmol/min) vs. time at 650 °C and S/C=3, calculated with Eq. (4) (b) Percent extent of NiO reduction (α) in same conditions by rate integration, capped at 100% due to residual rate error (c) elimination of residual rate error by using X_{bio}=1 in Eq. (4) for acetic acid. (b) and (c) have matching y axis tickmarks (same scale).

to spherical particle volume of diameter 0.12 cm, and ϵ refers to stoichiometric moles of NiO reduced by 1 mol of bio-compound according to the prevalent reduction reaction. We later show in Section 3.3 that the prevalent reduction reaction was R1. Thus, according to R1, for bio-compound of elementary molar formula $C_iH_jO_l$, ε was $(2i+0.5j-l)$, e.g. for ethanol, ε was 6 (mol of NiO reduced per mol of ethanol). Table 2 shows that the values of $W_{bio,r}$ were in all cases roughly two orders of magnitude greater than the observed chemical consumption rate $r_{bio,ext}$. Therefore, the external mass transfer limitation was considered negligible for the 5 bio-compounds and methane.

3.2.2. Internal mass transfer

The internal diffusion (intraphase) resistance may play an important role in controlling global reaction rate when the gaseous reactant needs to penetrate the pores of solid material to reach the solid particles of NiO. The experiment at S/C of 3 using ethanol as bio-compound was repeated using particle sizes of 0.1 mm instead of 1.2 mm using 2 g of catalyst load. The same reduction rate profile with time on stream was obtained, which indicated that internal diffusion rate was not rate limiting. We show later in Section 3.4 that ethanol exhibited the fastest apparent NiO reduction rate of all the bio-compounds (not counting CH_4) at temperatures 550–750 °C and S/C of 3 (except acetone at 550 °C), in same conditions. In addition, an estimation of the Thiele modulus at 650 °C for all the feed mixtures was carried out. Thiele modulus is given by Eq. (10), and represents the root square of the ratio of chemical rate to diffusive rate inside a porous catalyst [33]. In absence of internal diffusion limitation, Thiele modulus $\Phi_n \ll 1$, as the internal diffusion rate far exceeds that of chemical reaction:

$$\Phi_n{}^2 = \frac{\left(0.5d_p\right)^2 \text{rate}}{D_e\left(C_{bio,S}-0\right)} \tag{10}$$

In Eq. (10), 'rate' is the rate of bio-compound consumption (in mol m^{-3} s^{-1}), determined later in the kinetic model fitting Section 3.5.2 via dividing the modelled rate of NiO reduction by ε. This calculation was determined at the point of NiO conversion (α) of 0.5, which roughly also corresponded to X_{bio} = 0.5, marking the upper limit over which the data was fitted in the kinetic modelling section. These conditions matched the fastest reduction rate as will be seen in Section 3.4, thus also largest Φ_n. The effective diffusivity D_e was estimated using Eq. (11):

$$D_e = \frac{D_{bio,N_2}\Phi_p\sigma_C}{\tau} \tag{11}$$

Here we assumed a typical value of constriction factor σ_C0.8 [33], and used the tortuosity τ = 3.54 and particle porosity Φ_p = 0.59 of a similar α-alumina supported steam reforming Ni catalyst [34] to determine D_e. Values of D_e, rate, $C_{bio,S}$ and of the Thiele Modulus Φ_n have been compiled in Table 2 for all the bio-compound experiments at 650 °C at maximum chemical rate conditions. These confirmed that, with all the values of Φ_n having been found to be smaller than 0.02, internal diffusion limitations were deemed negligible in the conditions for which the kinetic model and rate constants parameters were derived.

3.3. Conversions and products yields via carbon and hydrogen balances

Fig. 2(a-d) represents the main outputs profiles with time on stream at the onset of gas evolution from the gas analysers for three of the bio-compound reductants tested (ethanol, acetone and furfural), at conditions of 650 °C, ~1.174 mmol/min of C in the feed, at S/C of 3, for purposes of clarity. Profiles for acetic acid can be found in [35]. The percent conversions of bio-compound and of steam according to Eqs. (2)–(3) are shown in Fig. 2a. Fig. 2b and c plot the carbon-containing gas products yields (CO and CO_2) and hydrogen-containing gas products yields (H_2 and CH_4) respectively, in units of moles of product per mole of carbon in the feed, and calculated as ratios of molar rates. Conversion of the bio-compound to CO_2, CO and CH_4, (no C2 or C3 gases detected) was able to reach nearly 100%, thus ruling out significant carbon accumulation at the end of this first very reactive phase. Considered together, the negative steam conversion and CO_2 yield, accompanied by minimal CO, H_2 and CH_4 yields during the first 150 s of time on stream, indicated that reactions of type R1 (reduction with production of CO_2 and H_2O, i.e. chemical looping combustion) were the net dominant global reactions. Fig. 2d, which plots the ratio of yields of H_2O yield to CO_2 further confirmed that in the first 150 s of time on stream, this ratio closely approximated the stoichiometric ratio $(0.5j/i)$ of R1 for the relevant bio-compound $C_iH_jO_l$: e.g. 1.5 for ethanol, 1 for acetone and 0.4 for furfural. Thus global reactions of type R1 using the reactant bio-compound as the reductant rather than intermediates, were the net contributors to the first phase of bio-compound conversion, whilst R2, R3 and R4 and carbon accumulation were negligible during this first phase. The identification of R1 with the bio-compound reductant as the sole active net global reaction during this period allowed us to relate the NiO reduction rate to a bio-compound consumption rate via the value of ε in the assessment of mass transfer limitations (external and internal).

3.4. Estimation of reduction rate and reduction extent

On the basis of oxygen balance (Eq. (4)), the rate of NiO reduction with various reductants was estimated. These calculations made no assumptions on the reactions at work because they were purely based on elemental balances. Reduction rate profiles with respect to time are shown in Fig. 3a. The reduction was completed in the first 250 s of each experiment. Some bio-compounds such as ethanol and acetic acid reached 100% reduction more quickly. Maxima of extent of NiO reduction (α_{max}), calculated after integration of rates with time on stream and compared to the initial molar content of NiO (4.82×10^{-3} mol), shown in Fig. 3b is corroborated by XRD characterization as discussed in Section 3.1. A small residual error of reduction rate was observed after 360 s in all the bio-compounds reduction rate curve but not in the NiO reduction rate under CH_4. If a catalyst pre-reduced in hydrogen was used in the experimental process instead of the fresh catalyst, a similar residual error was still seen. The residual error is attributed here to the underestimation of oxygen contribution from bio-compounds to oxygen-containing products, e.g. intermediate products in condensable phases.These unquantified products did not appear in Eq. (4) since they were not represented in the bio-compound conversion term X_{bio}. To assess the effect on the reduction rate of the residual rate error, which results in extents of NiO reduction exceeding 100% with time on stream, we replaced the X_{bio} term in Eq.(4) by the value of 1. This assumes that all the oxygen in the bio-compound is converted to product from the start of the experiment. The result is illustrated in Fig. 3c for acetic acid at 650 °C at S/C of 2 with 2 g of catalyst. The case of acetic acid represents a feedstock bio-compound of highest O/C content, and highest residual rate error to maximum reduction rate ratio of all the compounds (Fig. 3a). It can be observed from Fig. 3c that the extent of reduction (α) curve vs. time was unaffected by inaccuracy in oxygen contribution from the bio-compound conversion term in Eq. (4) for a large range of α. A discrepancy between the α vs. time curve, calculated with X_{bio} derived from Eq. (2), and the α vs. time curve derived assuming $X_{bio} = 1$, was only observed for α values beyond 68%, ie. largely above the upper limit for which our kinetic data was later fitted. Furthermore, the α vs. time curve obtained assuming $X_{bio} = 1$ very nicely reached 100% asymptotically, strongly suggesting that our interpretation of the reasons behind the residual rate error was correct, i.e. that all the oxygen in the bio-compound was quickly converted to product, even if this product was not CO, CO_2, or H_2O. Thus, even if carbonaceous product or other condensed phase oxygenates had been net-generated during the reduction, the oxygen balance reflected in Eq.(4), which allows the reduction rate of NiO to be estimated, would have not been affected in the region of $\alpha < 0.5$.

3.5. Kinetic modelling of NiO reduction by bio-compounds

3.5.1. Selection of conversion range for kinetic modelling

Thermodynamic calculations (to be published) indicated that the carbon formation during NiO reduction with the bio-compounds depends on the availability of NiO in the reaction system. Cho et al. [8] observed experimentally that the carbon deposition was not significant until 80% NiO was reduced during chemical looping combustion of CH_4. The data within the conversion fraction α of 0-0.5 of the present study was used as input for kinetics modelling. Kinetic analysis based on a selected conversion range is often used in the literature [36,37] due to the difficulty in obtaining kinetic data in a full conversion range. For example, for the reduction of metal oxide with CH_4, kinetic data are obtained normally by recording the mass change of solid sample during reduction.

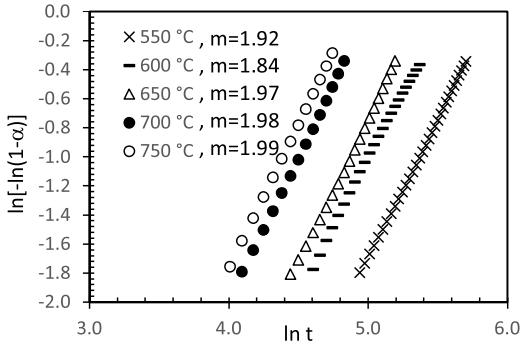

Fig. 4. Plots of $\ln[-\ln(1-\alpha)]$ vs. $\ln t$ for the reduction of NiO catalyst with furfural (S/C=3) at different temperatures (between 550 and 750 °C). Values of m close to 2 indicate A2 model (Avrami–Erofeyev's nucleation and nuclei growth with 2D nuclei shape).

3.5.2. Model fitting

Generally, kinetics of solid state reaction can be expressed as Eq. (12) or its integral form Eq. (13), where α is the conversion fraction of reactant in time t (we called this the reduction extent in 3.4), k is the reaction rate constant (here termed $k_{NiO \rightarrow Ni}$), and f(α) or g(α) represent the reaction mechanism. The kinetic models tend to fall into three groups [5,36,38]: (1) diffusion models, (2) geometrical contraction models and (3) nucleation and nuclei growth models.

$$\frac{d\alpha}{dt} = k \times f(\alpha) \tag{12}$$

$$g(\alpha) = \int \frac{d\alpha}{f(\alpha)} = k \times t \tag{13}$$

$$\ln(-\ln(1-\alpha)) = ln(\beta) + m \times ln(t) \tag{14}$$

Hancock and Sharp [38] developed a convenient method for kinetic model-fitting of isothermal solid state reactions (Eq. (14)) where β is a constant, m depends on the geometry of reactant particles and the reaction mechanism. The kinetic model gives rise to approximately linear plots of $\ln[-\ln(1-\alpha)]$ vs. $\ln(t)$ if the range of α is limited to 0.15–0.5. The gradient m of such plots could be used to help select the most suitable kinetic model. Theoretically, the m value is located around 0.5 for diffusion controlled reactions, around 1.0 for geometrical contraction controlled and first-order reactions, and from 1.0 to 3.0 for nucleation and nuclei growth controlled reactions (1 corresponding to rod shape nuclei, 2 to disc shape, 3 to spherical, and >3 cases (e.g. 4 or 5) where spherical nucleation and nuclei growth are concurrent).

In the present study, the Hancock-Sharp method was employed. The m values varied with reaction temperatures and S/C used but were located between 1.0 and 2.0 for temperatures in the range 550–750 °C. Plots of ln[-ln(1-α)] vs. ln t for NiO reduction with furfural (S/C=3) at different temperatures are shown in Fig. 4 as an example. When using the other bio-compounds to reduce NiO catalyst, similar linear plots were obtained and their m values are listed in Table 3. For the NiO reduction with furfural or CH_4, the m values hardly changed with temperature, and were all close to 2.00, indicating a two-dimensional nuclei growth mechanism (A2 model). Values for m obtained from reduction using acetic acid, ethanol or acetone increased gradually as the temperature rose from 550 °C to 650 °C, although in majority were larger than 1, still suggesting Avrami–Erofeyev models of changing nucleus shape. Within the temperature range of 650–750 °C, the reduction was an isokinetic process, indicated by a negligible variation in the m value. It was found that only the initial stage of reduction at 550 °C obeyed the A2 model. Therefore, the following A2 model fit was performed in the conversion range of 0-0.20 for 550 °C whereas the conversion range of 0–0.5 was used for the other four temperatures (600–750 °C).

Table 3
The m values in Hancock and Sharp's method (Eq. (14)) obtained at reduction temperatures between 550 °C and 750 °C.

Reductant	550 °C	600 °C	650 °C	700 °C	750 °C
acetic acid	1.34	1.63	1.78	1.73	1.75
ethanol	0.99	1.56	1.89	1.90	1.87
acetone	1.45	1.69	1.88	1.91	1.87
CH_4	1.83	1.97	1.94	1.95	1.96
furfural	1.92	1.84	1.97	1.98	1.99
glucose	1.20	1.52	1.57	1.51	1.53

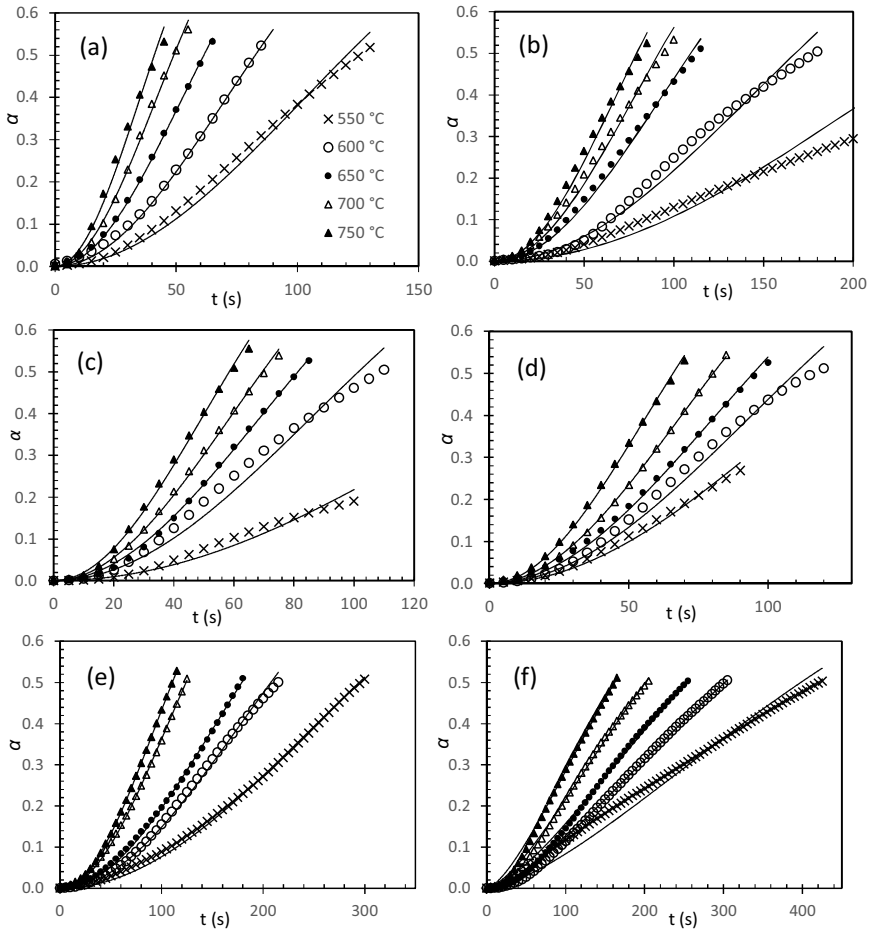

Fig. 5. Comparison between the experimental extent of reduction α vs. time and the curve predicted using A2 model for the reduction of NiO catalyst with (a) CH_4, (b) acetic acid, (c) ethanol, (d) acetone, (e) furfural and (f) A1.5 model with glucose (S/C=6 for glucose and S/C=3 for the other bio-compounds). Scatter points are experimental points, lines are associated model fits.

Glucose was the exception to all the bio-compounds studied, which had m values around 1.5. The use of Avrami–Erofeyev equation with non-integral m value (m = 1.34) to fit the conversion curve observed from NiO reduction with H_2 has been reported in the literature [2,39]. In this study, Avrami–Erofeyev equation with m = 1.5 (denoted as A1.5) was used to fit the kinetic data obtained from NiO reduction with glucose solution. Non integer m values between 1 and 3 are indicative of irregular shaped nuclei.

Once the kinetic model was determined, the rate constant $k_{NiO\rightarrow Ni}$ of the NiO reduction reaction could be derived from experimental data (fractional conversion α vs. time) by two methods. One was to linearly fit the plot of $[-\ln(1-\alpha)]^{1/m}$ vs. t, and obtain $k_{NiO\rightarrow Ni}$ from the slope [40]. The other was to fit the plot of α vs. t with the exponential function

$$\alpha = 1 - \exp[-((k_{NiO\rightarrow Ni}t)^m)] \quad (15)$$

In both methods, m values of 1.5 and 2 were used for glucose and for the all the other bio-compounds, respectively. The exponential fit method was employed in this work. A good agreement between the experimental data and theoretical model was achieved, as shown in Fig. 5 and through the correlation coefficient R^2's closeness to 1 (average R^2 over 30 experiments = 0.9917, minimum R^2 = 0.961).

3.5.3. Apparent activation energy and pre-exponential factor

The reduction rate constants $k_{NiO\rightarrow Ni}$ obtained at different temperatures were plotted into Arrhenius plots (Fig. 6). The apparent activation energies E_a, were derived from the slope of the Arrhenius plots (Eq. (16)), and are listed in Table 4.

$$\ln k_{NiO\rightarrow Ni} = \ln A - \frac{E_a}{RT} \quad (16)$$

It was found that the values of E_a of NiO reduction with different reductants were close to each other and located at around 30–40 kJ/mol of NiO. This suggested that the influence of temperature on the reduction rate constant was similar for the different

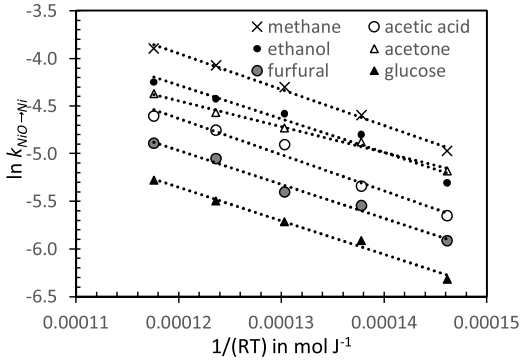

Fig. 6. Arrhenius plots of rate constants $k_{NiO\to Ni}$ of NiO reduction with bio-compounds as well as methane at S/C=3 (S/C=6 for glucose).

Table 4
Estimated kinetic parameters apparent kinetic energy E_a and pre-exponential factor A for NiO reduction with different reductants, using linear fit of Eq. (16), goodness of fit expressed by R^2's closeness to 1.

Reductants	E_a (kJ/mol NiO)	A (s^{-1})	R^2
CH_4	38 ± 2	1.79	0.9933
ethanol	35 ± 4	0.96	0.9562
acetone	27 ± 2	0.30	0.9905
acetic acid	38 ± 4	0.92	0.9733
furfural	36 ± 3	0.50	0.9847
glucose	35 ± 2	0.32	0.9896

bio-compounds. An approximate activation energy (53.5 kJ/mol) was observed for the reduction of NiO/α-Al_2O_3 with CH_4 in the absence of steam using Avrami–Erofeyev model with $m = 1$ by Hossain and Lasa [30].

The relative position of these Arrhenius plots indicates that the rate constants can be ordered as follows: CH_4 > ethanol ≈ acetone > acetic acid > furfural > glucose. Table 5 compares the rate constants of the NiO reduction with bio-compounds to those with ethanol for the temperature range 550–750 °C. The pre-exponential factor A represents the probability that the reducing species encountering a NiO nucleus or particle will achieve reaction. Table 4 indicates CH_4 had by far the largest A value. Table 5 further compares magnitudes of reduction rate constants by listing their ratios relative to those of ethanol at the different temperatures studied, as well as ratio averages of all temperatures. Clear differences between bio-compounds are observed over the 550–750 °C range, with acetic acid's being approximately 2/3 the rate constant of ethanol, whereas furfural's was ½, and glucose's 1/3. Acetone's was similar to ethanol's, while methane's was 4/3. Further characterization of the species adsorbed on the catalyst surface (e.g. X-ray photoelectron spectroscopy, XPS) is necessary in order to understand the difference arising from the different bio-compounds.

3.6. Effects of steam content on reduction rate

The influence of water on metal oxide reduction has been investigated in the literature. Gardner [40] observed that the presence of water vapour in the ambient gas considerably lowered the reduction rate of SiO_2 by H_2. He explained that surface activity of SiO_2 was decreased by the interaction between SiO_2 and water (formation of Si-OH) and hence fewer sites were available for the adsorption of H_2. Richardson et al. [29,41] suggested that the adsorbed H_2O molecules decreased the reducibility of NiO/Al_2O_3 catalyst by slowing down the diffusion of metallic Ni atoms to appropriate nucleation sites. However, Abad et al. and Garcia-Labiano et al. [42,43] found that the presence of H_2O or CO_2 had no effect on the reduction rate of supported metal oxide with CH_4, CO or H_2 as reductant.

In this study, the reduction rate constant $k_{NiO\to Ni}$ at 650 °C varied with the water content present in the reaction system as shown in Fig. 7(a). In the absence of water (S/C=0), a low rate constant was obtained. As the S/C rose, the rate constant increased first, and then decreased. This decrease became less pronounced at higher S/C. In general, the maximum reduction rate constants were obtained in the S/C range of 1–2. For glucose, the S/C studied in this work only covered from 4.5 to 9 due to the limitation on its solubility. Therefore, only the stages of decrease and levelling off were observed with increasing S/C.

Table 5
Ratios of rate constants $k_{NiO\to Ni}$ of reduction of NiO to Ni with bio-compounds with respect to rate constant of reduction with ethanol. The reduction rate constants of acetic acid, ethanol, acetone, furfural, glucose and CH_4 are denoted as k_1, k_2, k_3, k_4, k_5 and k_6, respectively.

Temperature (°C)	acetic acid k_1/k_2	acetone k_3/k_2	furfural k_4/k_2	glucose k_5/k_2	CH_4 k_6/k_2
550	0.706	1.135	0.544	0.363	1.395
600	0.585	0.925	0.475	0.329	1.228
650	0.722	0.859	0.439	0.322	1.324
700	0.717	0.865	0.534	0.342	1.418
750	0.702	0.887	0.526	0.358	1.427
average	0.7	0.93	0.5	0.35	1.36

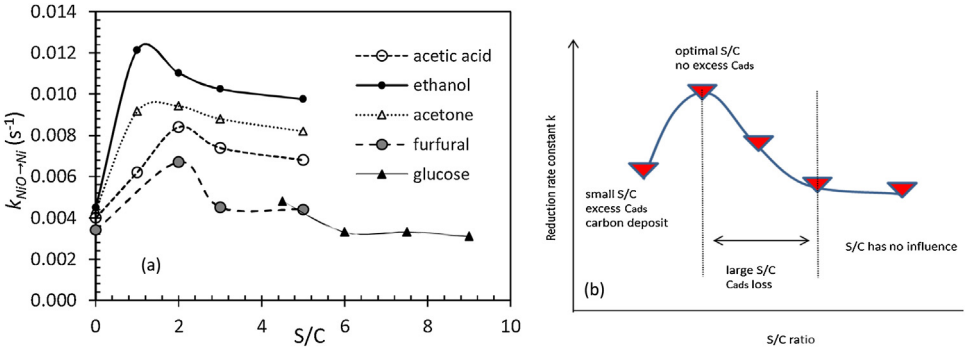

Fig. 7. (a) Reduction rate constant $k_{NiO\to Ni}$ at 650 °C vs. S/C for individual bio-compounds, (b) reduction rate constant vs. S/C, general case of bio-compounds.

According to the reduction mechanism proposed in [17], the presence of water has two opposite effects on the reduction. Firstly, the adsorbed H_2O molecules slow down the reduction by scavenging radicals (i.e. potential reducing species), and limiting the migration of Ni atoms to nucleation sites. In addition, an appropriate amount of H_2O could suppress the deposition of carbon by promoting steam gasification. As a result, the dissociation of bio-compounds on Ni sites (the initial step of reduction) is not affected. Which effect is dominant depends on the reaction condition. Fig. 7(b) illustrates the effect of S/C on the adsorbed carbon radicals (C_{ads}), which explains the typical profile of rate constant vs. S/C observed in experiments at 650 °C for the bio-compounds studied.

The maximum reduction rate constant could be obtained when the amount of water (optimal S/C) is just enough to gasify the excess C_{ads} and not consume those that are supposed to reduce NiO. The optimal S/C varies with bio-compounds, which may be attributed to the different activities of carbon radicals produced from different sources as well as the consumption rate of carbon radicals (i.e. reduction rate). It should be noted that the optimal S/C range for reduction kinetics was below the S/C commonly used for steam reforming (e.g. S/C=2-3).

4. Conclusions

NiO catalyst could be completely reduced by ethanol at 650 °C and by acetic acid, acetone, furfural, glucose and CH_4 at 550 °C. Reduction kinetics matched the two-dimensional nucleation and nuclei growth model (A2) except for glucose (A1.5). The apparent activation energies of NiO reduction to Ni were all located in the range of 30–40 kJ/mol. Their rate constants decreased following CH_4 > ethanol ≈ acetone > acetic acid > furfural > glucose. Feed steam content also affected reduction rate. The rate constant peaked at S/C 1–2. Ethanol exhibited a larger reduction rate constant and a lower optimal S/C, probably because its carbon radicals had a higher activity.

Acknowledgements

We wish to thank EPSRC (Consortium Supergen XIV "Delivery of Sustainable Hydrogen", EP/G01244X/1) for financial support (consumables), The University of Leeds and China Scholarship Council for CSC-Leeds University Scholarship for Dr Feng Cheng, and Johnson Matthey Plc (Jim Abbott) for catalyst materials. Supporting data for this article can be found at http://doi.org/10.5518/91.

References

[1] O. Ostrovski, G.Q. Zhang, AIChE J. 52 (2006) 300–310.
[2] J.T. Richardson, R. Scates, M.V. Twigg, Appl. Catal. A: Gen. 246 (2003) 137–150.
[3] E.B.H. Quah, C.Z. Li, Appl. Catal. A: Gen. 258 (2004) 63–71.
[4] S.S.A. Syed-Hassan, C.Z. Li, Appl. Catal. A: Gen. 398 (2011) 187–194.
[5] A. Khawam, D.R. Flanagan, J. Phys. Chem. B 110 (2006) 17315–17328.
[6] M. Ryden, M. Johansson, A. Lyngfelt, T. Mattisson, Energy Environ. Sci. 2 (2009) 970–981.
[7] M.M. Hossain, D. Lopez, J. Herrera, H.I. de Lasa, Catal. Today 143 (2009) 179–186.
[8] P. Cho, T. Mattisson, A. Lyngfelt, Ind. Eng. Chem. Res. 44 (2005) 668–676.
[9] L.F. de Diego, M. Ortiz, F. Garcia-Labiano, J. Adanez, A. Abad, P. Gayan, J. Power Sourc. 192 (2009) 27–34.
[10] M.M. Hossain, M.R. Quddus, H.I. de Lasa, Ind. Eng. Chem. Res. 49 (2010) 11009–11017.
[11] M.M. Hossain, H.I. de Lasa, Chem. Eng. Sci. 65 (2010) 98–106.
[12] A. Lea-Langton, R. Md Zin, V. Dupont, M.V. Twigg, Int. J. Hydrogen Energy 37 (2012) 2037–2043.
[13] R.M. Zin, A.B. Ross, J.M. Jones, V. Dupont, Bioresour. Technol. 176 (2015) 257–266.
[14] B.L. Dou, Y.C. Song, C. Wang, H.S. Chen, M.J. Yang, Y.J. Xu, Appl. Energy 130 (2014) 342–349.
[15] P. Pimenidou, G. Rickett, V. Dupont, M.V. Twigg, Bioresour. Technol. 101 (2010) 6389–6397.
[16] N. Giannakeas, A. Lea-Langton, V. Dupont, M.V. Twigg, Appl. Catal. B: Environ. 126 (2012) 249–257.
[17] F. Cheng, V. Dupont, Int. J. Hydrogen Energy 38 (2013) 15160–15172.
[18] R. Md Zin, A. Lea-Langton, V. Dupont, M.V. Twigg, Int. J. Hydrogen Energy 37 (2012) 10627–10638.
[19] X. Hu, G. Lu, Appl. Catal. B: Environ. 88 (2009) 376–385.
[20] M. Marquevich, S. Czernik, E. Chornet, D. Montané, Energy Fuels 13 (1999) 1160–1166.
[21] D.R. Goodman, Handling and using catalysts in the plant, in: M.V. Twigg (Ed.), Catalyst Handbook, Manson Publishing Limited, London, 1996.
[22] L. McCusker, R. Von Dreele, D. Cox, D. Louer, P. Scardi, J. Appl. Crystallogr. 32 (1999) 36–50.
[23] R. Molinder, T. Comyn, N. Hondow, J. Parker, V. Dupont, Energy Environ. Sci. 5 (2012) 8958–8969.
[24] A.N. Rollinson, G.L. Rickett, A. Lea-Langton, V. Dupont, M.V. Twigg, Appl. Catal. B: Environ. 106 (2011) 304–315.
[25] W.-P. Dow, Y.-P. Wang, T.-J. Huang, J. Catal. 160 (1996) 155–170.
[26] D.E. Ridler, V. Twigg, Steam reforming, in: M.V. Twigg (Ed.), Catalyst Handbook, Manson Publishing Limited, London, 1996.
[27] A.C. Basagiannis, X.E. Verykios, Appl. Catal. A: Gen. 308 (2006) 182–193.
[28] Q. Zafar, A. Abad, T. Mattisson, B. Gevert, Energy Fuels 21 (2007) 610–618.
[29] J. Richardson, R. Scates, M. Twigg, Appl. Catal. A: Gen. 267 (2004) 35–46.
[30] M.M. Hossain, H.I. de Lasa, AIChE J. 53 (2007) 1817–1829.
[31] W.E. Ranz, W.R. Marshall, Chem. Eng. Prog. 48 (1952) 247–253.
[32] E.N. Fuller, P.D. Schettler, C. Giddings, J. Ind. Eng. Chem. 58 (1966) 19–27.
[33] H.S. Fogler, Diffusion and reaction, in: Elements of Chemical Reaction Engineering, Pearson Eduction Inc., 2006, Online version, Chapter 12.
[34] J. Xu, G.F. Froment, AIChE J. 35 (1989) 97–103.
[35] F. Cheng, V. Dupont, Int. J. Hydrogen Energy 38 (2013) 15160–15172.
[36] K.S. Go, S.R. Son, S.D. Kim, Int. J. Hydrogen Energy 33 (2008) 5986–5995.
[37] H.J. Ryu, G.T. An, Korean J. Chem. Eng. 24 (2007) 527–531.
[38] J. Hancock, J. Sharp, J. Am. Ceram. Soc. 55 (1972) 74–77.
[39] A.F. Benton, J. Am. Chem. Soc. 46 (1924) 2728–2737.
[40] R.A. Gardner, J. Solid State Chem. 9 (1974) 336–344.
[41] J. Richardson, M. Lei, B. Turk, K. Forster, M.V. Twigg, Appl. Catal. A: Gen. 110 (1994) 217–237.
[42] F. Garcia-Labiano, L. De Diego, J. Adánez, A. Abad, P. Gayán, Ind. Eng. Chem. Res. 43 (2004) 8168–8177.
[43] A. Abad, F. García-Labiano, L.F. de Diego, P. Gayán, J. Adánez, Energy Fuels 21 (2007) 1843–1853.